Chemistry–A European Journal

Research Article
doi.org/10.1002/chem.202300459

Chemistry Europe
European Chemical Societies Publishing

www.chemeurj.org

Special Collection

Transformation of the *cyclo*-P_5 Middle Deck in [(Cp*Fe)(Cp'''Co)(μ,η^5:η^4-P_5)] upon Functionalization – A Comprehensive Study of Reactivity

Sabrina B. Dinauer,[a] Martin Piesch,[a] Robert Szlosek,[a] Michael Seidl,[a] Gábor Balázs,[a] and Manfred Scheer*[a]

Dedicated to Professor Dietmar Stalke on the occasion of his 65th birthday

Abstract: The heterobimetallic triple-decker complex [(Cp*Fe)(Cp'''Co)(μ,η^5:η^4-P_5)] (**1**) was functionalized by main group nucleophiles and subsequently electrophilically quenched or oxidized. Reacting **1** with group 14 nucleophiles revealed different organo-substituted P_5R middle-decks depending on the steric and electronic effects of the used alkali metal organyls (**2**: R = tBu; **3**: R = Me). Further, with group 15 nucleophiles, the first structural characterized monosubstituted complexes with phosphanides could be obtained as P_5 ligands containing exocyclic {PR_2} units (**4**: R = Cy, H; **5**: R = Ph). These monoanionic complexes **2–5** were isolated and subsequent electrophilic quenching revealed novel types of neutral functionalized polyphosphorus complexes. These complexes bear formal chains of $P_5R'R''$ (**6**: R′ = tBu, R′ = Me) in a 1,3-disubstitution pattern or $P_6R'R''R'''$ units (**7**: R′ = Cy, R″ = H, R‴ = Me; **8**: R′ = Me, R″ = Ph, R‴ = Me) in a 1,1,3-substitution as middle-decks stabilized by one {Cp'''Co} and one {Cp*Fe} fragment. One-electron oxidation of **2**, **3** or **5** by $AgBF_4$ gave access to paramagnetic triple-decker complexes bearing P_5R middle-decks in various coordination fashions (R = *t*Bu (**10**), R = PPh_2 (**12**)). Interestingly, for R = Me (**11**), a dimerization is observed revealing a diamagnetic tetranuclear cluster containing a unique dihydrofulvalene-type $P_{10}R_2$ ligand. All complexes were characterized by crystallographic and spectroscopic methods (EPR, multinuclear NMR and mass spectrometry) and their electronic structures were elucidated by DFT calculations.

Introduction

The controlled transformation of white phosphorus (P_4)[1,2,3] and yellow arsenic (As_4)[4] by main group elements or transition metals spans a wide range of research as outlined in several reviews. Stepwise cleavage of the E–E bonds in the E_4 tetrahedron can be mediated by main group or transition metal fragments providing access to a plethora of versatile compounds featuring polypnictogen (E_n) substituents or ligands.[2–5,6] These conversions of P_4 by transition metal (TM) complexes represent the first step towards the formation of polyphosphorus compounds within the respective coordination sphere. Further functionalization of the P_n units by organic substituents leads to organophosphorus ligands in a second step, which remains less explored than the first step.[5,7] A first selective and direct functionalization of a *cyclo*-P_n end-deck ligand was achieved by Peruzzini et al. in 1986 via electrophilic alkylation of [{$MeC(CH_2PPh_2)_3$}M(η^3-P_3)] (Scheme 1a; **I**, M = Co–Ir) with MeOTf or [Me_3O][BF_4] yielding [{$MeC(CH_2PPh_2)_3$}M(η^3-P_3Me)]X (**III**, X = BF_4^-, OTf).[8] Further, the reactivity of *cyclo*-P_3 complexes towards main group nucleophiles was investigated by our group using the nickel complex [Cp'''Ni(η^3-P_3)] (**II**, Scheme 1a).[9] Depending on the choice of the nucleophile, a substituted cyclic P_3R ligand was generated in the reaction with $LiNMe_2$ (**IV**). In contrast, the reaction of **II** with $LiPPh_2$ gives the analogous anionic P_3R-containing complex, which reacts in solution with another equivalent of **II** leading to a bicyclic P_6 ligand.[9] Furthermore, *cyclo*-P_4 ligands in the coordination sphere of Fe were functionalized with boron compounds (**VII**, Scheme 1b).[10] Apart from that, the reactivity of the *cyclo*-P_4 ligand in [Cp'''Co(η^4-P_4)] was explored by our group towards carbon-based nucleophiles with endo-substituted tetraphosphido complexes [Cp'''Co(η^3-P_4R)]$^-$ (**VIII**, R = *t*Bu, CH_2SiMe_3, Scheme 1b) being isolated.[11] In addition, the reactivity of the anionic *cyclo*-P_3 complex [Cp'''Co(η^3-P_3)]$^-$ towards chlorophosphines was analyzed yielding complexes revealing finally P_3-{PR_2}-type ligands.[12] Via cationic functionalization of the *cyclo*-P_5 end-deck in [Cp*Fe(η^5-P_5)] (**IX**), an unprecedented diversity of p-block

[a] S. B. Dinauer, Dr. M. Piesch, R. Szlosek, Dr. M. Seidl, Dr. G. Balázs, Prof. Dr. M. Scheer
Institute of Inorganic Chemistry
University of Regensburg, 93040 Regensburg (Germany)
E-mail: manfred.scheer@chemie.uni-regensburg.de
Homepage: http://www.uni-regensburg.de/chemie-pharmazie/anorganische-chemie-scheer/startseite/index.html

Supporting information for this article is available on the WWW under https://doi.org/10.1002/chem.202300459

Special Collection Part of a Special Collection on the p-block elements.

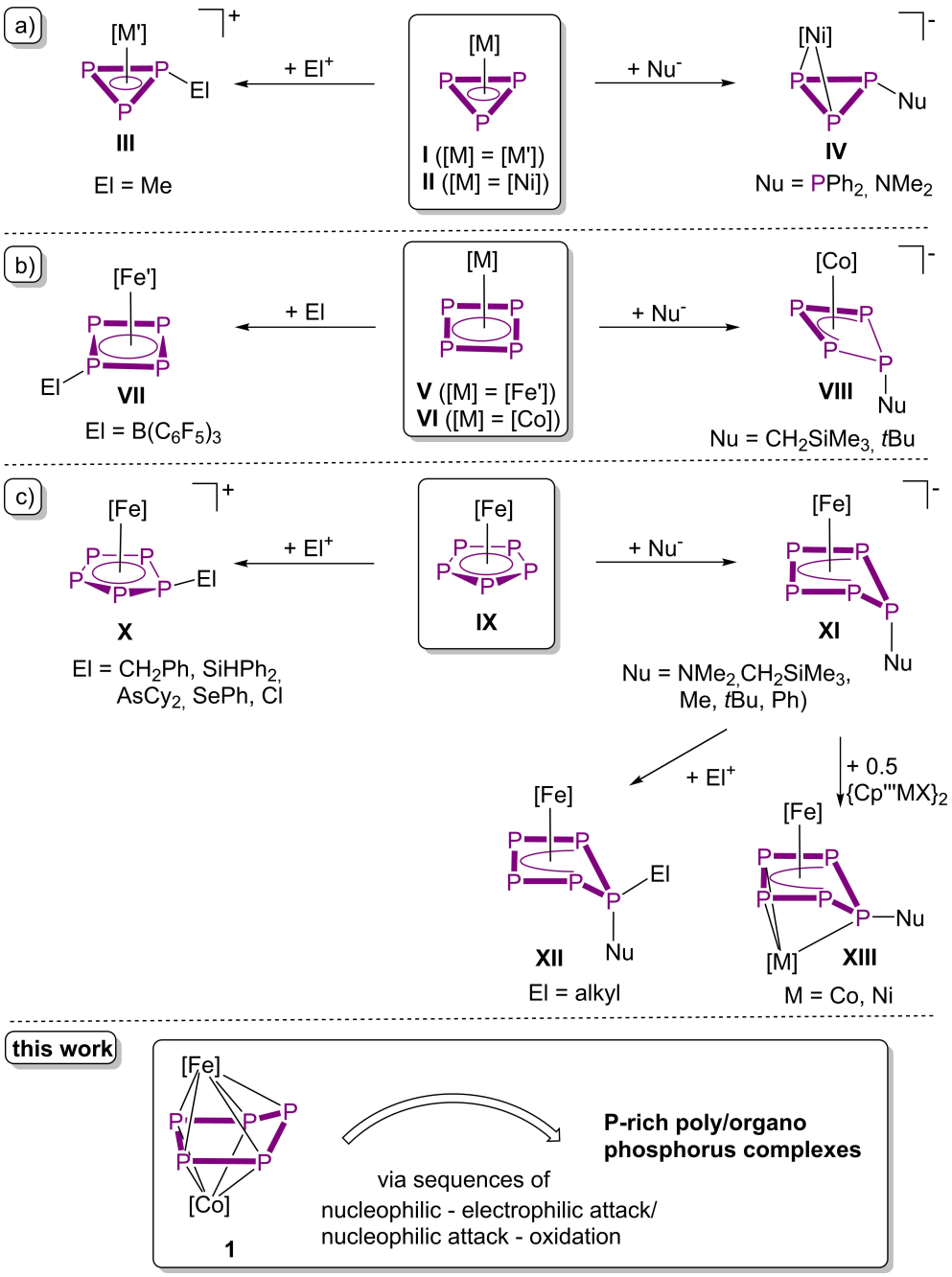

Scheme 1. Selected examples of neutral *cyclo*-P_n ($n = 3$-5) end-deck complexes and their functionalization by main group nucleophiles and electrophiles. a) Reactivity of the *cyclo*-P_3 complexes **I**, **II** towards electrophiles (**III**) and group 14 or 15 nucleophiles (**IV**). b) Synthesis of a neutral P-borylated complex **VII** and anionic P_4R complexes of the type **VIII**. c) Functionalization of [Cp*Fe(η^5-P_5)] (**IX**) with p-block electrophiles (**X**) or alkali metal organyls (**XI**) and subsequent quenching by carbon-centered electrophiles (**XII**) or transition metal halogen dimers (**XIII**) ([Ni] = [Cp'''Ni], [Fe] = [Cp*Fe], [Fe'] = [$^{Ph}PP_2^{Cy}$Fe], [Co] = [Cp'''Co], [M'] = [(triphos)M], triphos = $CH_3C\{CH_2P(C_6H_5)_2\}_3$, Cp''' = $C_5H_2{}^tBu_3$, Cp* = C_5Me_5, $^{Ph}PP_2^{Cy}$Fe = $PhP(CH_2CH_2PCy_2)$.

element moieties can be attached to the pnictogen ligand in which the aromatic character of the resulting pentaphosphole derivative is achieved (**X**, Scheme 1c).[13] Furthermore, upon nucleophilic functionalization of the *cyclo*-P_5 ligand in **IX**, the formation of P–C/P–N/P–P bonds giving complexes of the type **XI** was observed (Scheme 1c).[7,14] The mononuclear complexes **XI** bear the nucleophile in endo position leading to an envelope-type conformation of the *cyclo*-P_5R ligand coordinating in an η^4 fashion to [Cp*Fe]. Via this method, various alkyl and aryl substituents can be introduced into the phosphorus ligand.[7] Notably, in the reaction of **IX** and PH_2^-, the monoanionic product [Cp*Fe(η^4-P_5PH_2)]$^-$ is formed.[14] Subsequent quenching of **XI** with carbon-centred electrophiles provides access to 1,1-substituted complexes **XII**[7] (Scheme 1c) or monosubstituted triple-decker complexes **XIII** upon quenching with TM halides $\{Cp^RMX\}_2$.[15] Neutral complexes of the type **XII** show

a phosphonium ion-like character at the twofold substituted phosphorus atom, where the former electrophile is in exo position. Interestingly, **XII**-type complexes represent precursors for the synthesis of symmetrically/asymmetrically substituted organo-phosphines.[7]

A major drawback of this synthesis route is that the substitution pattern of **XII** is limited to 1,1 derivatives. Other selective twofold functionalizations of an end-deck *cyclo*-P_5 ligand have not been reported so far.[7] In contrast, by quenching of **XI** with transition metal dimers of the type $\{Cp^RMX\}_2$, the products are triple-decker complexes. The latter also show an envelope-type conformation of the P_5 middle deck, even though the electronic property of the introduced substituent has an impact on the bonding situation, that is, electron-donating substituents induce P–P bond elongation. However, via this synthetic route, only mono-functionalized P_5R middle decks could be obtained.[15] To the best of our knowledge, twofold functionalized P_5R_2 middle decks in triple-decker complexes are not known. In particular, the implementation of phosphorus nucleophiles in this type of chemistry, yielding mononuclear complexes, is not reported up to now. Recently, we reported the synthesis of the hetero-bimetallic triple decker complex [(Cp*Fe)(Cp'''Co)(μ,η^5:η^4-P_5)] (**1**) in the reaction of **IX** with the triple-decker complex [(Cp'''Co)$_2$(μ,η^4:η^4-C_7H_8)].[16] Via this route, the arsenic derivative **1'** was also synthesized. Due to the lower As–As bond energy, **1'** is less stable than **1** and can be selectively converted into complexes containing As_3 and As_{11} ligands.[17] In contrast, the lighter congener **1** proved to be more stable and thus should be a promising starting material for the functionalization by main group nucleophiles and electrophiles. The question arises whether a nucleophilic attack occurs at the phosphorus atom or the metal, and, if so, whether subsequent electrophilic quenching or oxidation preserve the structure of the initial P_5 unit providing also 1,1-disubstituted P_5 ligands or whether other substitution positions, that is, 1,2 or 1,3, of the electrophiles at the pnictogen ligand are possible. In addition, the formation of P–P bonds upon a nucleophilic attack may be stabilized by the 14 VE fragment {Cp'''Co} leading to more extended P_n units.

We herein report the reactivity of **1** towards different carbon- and phosphorus-centered nucleophiles leading to *catena*-P_5R middle-decks and exocyclic {PR_2} units, respectively. Further electrophilic quenching or oxidation of this anionic products by Ag salts give access to novel triple-decker complexes containing P_nR_x (n = 5, 6, 10; x = 1, 2, 3) middle decks paving the way for versatile organophosphorus ligands in transition metal triple decker complexes.

Results and Discussion

In order to evaluate the reactivity of [(Cp*Fe)(Cp'''Co)(μ,η^5:η^4-P_5)] (**1**) towards nucleophiles, computational studies at the BP86/def2-TVZP[18,19] level of theory were performed. The frontier molecular orbitals of **1** (Figure 1) reveal that both HOMO and LUMO orbitals are mainly located at the *cyclo*-P_5 ligand. In the case of the LUMO, the metals and the Cp* ligand show only a low contribution. Hence, nucleophilic attacks should be ligand-centered for **1**. The electrostatic potential surface of **1** (BP86-D3BJ/def2-TZVP level of theory) shows quite a delocalized negative charge at the *cyclo*-P_5 ligand, with a major contribution from the out-of-plane and adjacent P atoms (Figure 1c).

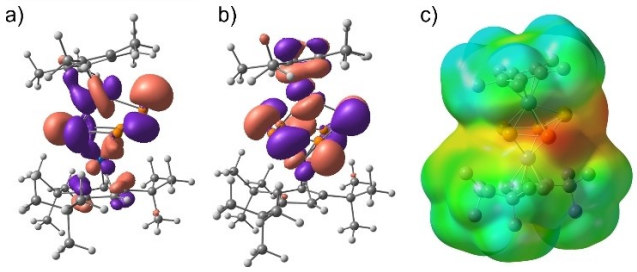

Figure 1. a) HOMO and b) LUMO orbitals of **1** at the BP86/def2-TVZP level of theory. c) Electrostatic potential mapped on electron density for **1**, Color code: blue = positive, red = negative.

The reaction of **1** with *t*BuLi and MeLi leads to the complexes [Li(2,2,2-crypt)][(Cp*Fe)(Cp'''Co)(μ,η^4:η^2:η^1-P_5R)] (**2**: R = *t*Bu; **3**: R = Me) in isolated yields of 26% and 76%, respectively (Scheme 2). The reaction of **1** with *t*BuLi leads to a complex reaction mixture,[20] the reaction of **1** with the MeLi is more selective and **3** is obtained in 76% yield (Scheme 2). In both complexes, the P_5R ligands are still in an envelope conformation. Depending on the size of the nucleophile, the smaller substituent (Me) is attached to a P atom which is in the plane of the P_5 envelope, while the *t*Bu substituent is attached to the out-of-plane P atom. Complex **3** shows dynamic behavior in solution at room temperature (see below). To check the steric influence of the carbon-based nucleophile on the structural motif of the resulting P_5R middle deck, **1** was also reacted with a nucleophile with a steric bulk in between Me and *t*Bu, that is, EtLi. In the ^{31}P NMR spectra, the clean formation of two products with an integral ratio of 1:1 is observed. The two sets of signals can be assigned to the Et-analogs of **2** and **3**, based on their similar chemical shifts and coupling constants (Figure 2). Extending the sterical demand to *sec*Bu (butan-2-ide), which is in between Et and *t*Bu, revealed the clean formation of one product according to the ^{31}P NMR spectrum of the crude reaction mixture. Regarding the set of multiplets and the integral ratio, the P_5(*sec*Bu) ligand is isostructural to the ligand in **2** (Figure 2). These results clearly show that the nature of the formed complexes is determined by the steric requirements of the nucleophile.

To broaden the scope of main group-based anionic nucleophiles, we changed the steric and electronic properties of the nucleophiles and switched to phosphorus-based nucleophiles. In principle, the formation of an additional P–P bond should enhance the stability of the corresponding polyphosphorus complexes and should provide novel substitution patterns. Accordingly, the reaction of **1** with alkali metal phosphanides (LiPCyH; $MPPh_2$, M = K, Li) yields the complexes [Li(12c4)$_2$][(Cp*Fe)(Cp'''Co)(μ,η^4:η^2:η^1-P_6CyH)] (**4**) and [K(2,2,2-

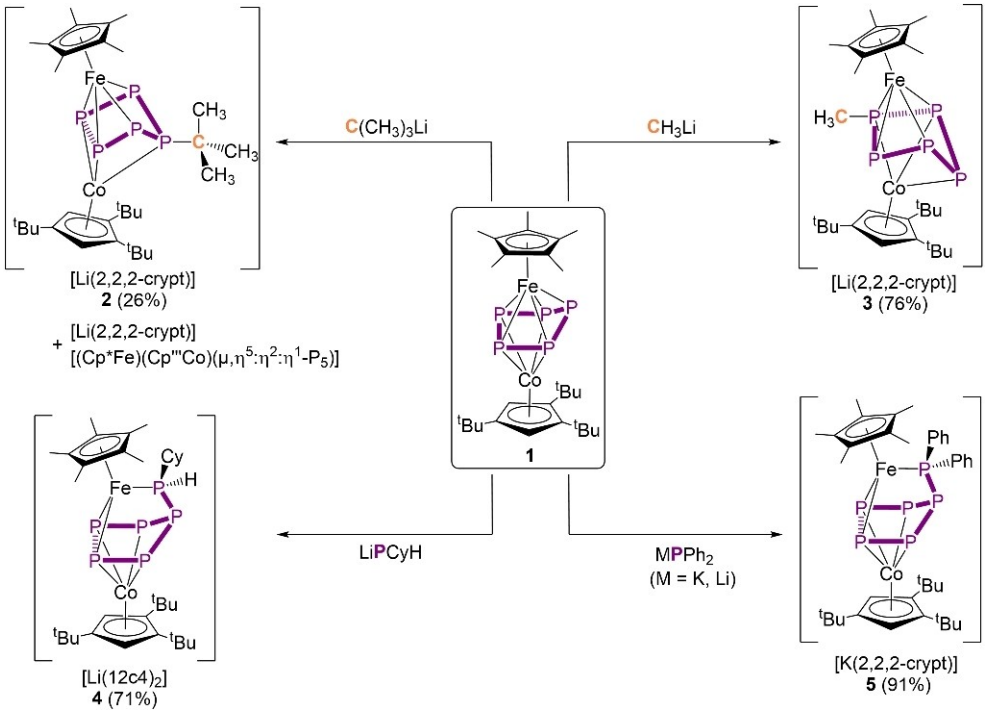

Scheme 2. Reactivity of the triple-decker complex **1** with different anionic carbon- and phosphorus-centered nucleophiles; reactions were carried out in thf at −80 °C (**2**, **3**, **5**) or r.t. (**4**) and 2,2,2-cryptand (1 equiv.) or 12c4 (2 equiv.) was added after 5 min; the yields in parentheses are for the isolated crystalline compounds.

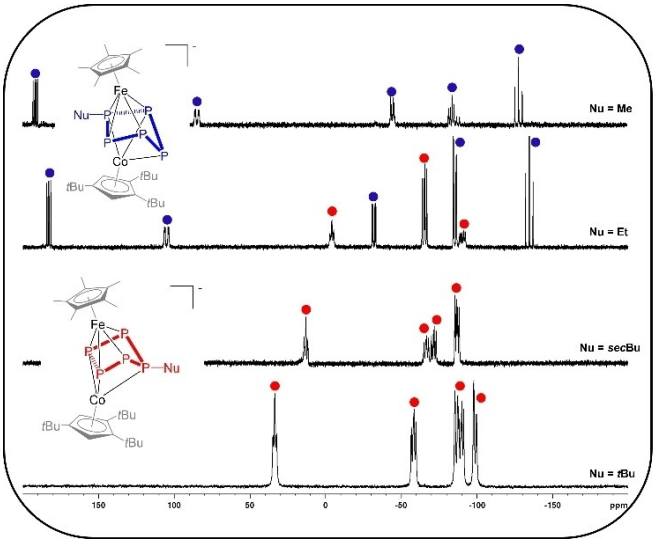

Figure 2. $^{31}P\{^{1}H\}$ NMR spectra of the reaction of **1** with MeLi (**2**), EtLi, *sec*BuLi and *t*BuLi (**3**), respectively, in thf-d_8 or in thf with C_6D_6 capillary at room temperature (Nu = Me, Et, *sec*Bu) or −80 °C (Nu = *t*Bu). Signal assignment in respect of the different P_5R motifs is according to the color code. For further details see Supporting Information.

crypt)][(Cp*Fe)(Cp'''Co)(μ,η^4:η^2:η^1-P_6Ph_2)] (**5**) in 71% and 91% yield, respectively (Scheme 2). Notably, complexes **4** and **5** represent the first structural characterized compounds containing a P_5-PR_2 unit, derived from a former P_5 ligand. In both compounds, P_6R_2 ligands built up by a folded P_5 ligand with an exocyclic {PR′R″} unit are present. The P_6R_2 ligand in **4** and **5** coordinates in an η^2:η^1 fashion to Fe and in an η^4 fashion to Co. By performing the reaction of **1** and LiPCyH at −80 °C, redox processes leading to $(CyP)_4$ and a second unknown compound could be observed. Thus, we performed the reaction of **1** and LiPCyH at r.t. for 15 min to enhance the nucleophilic reaction over the undesired redox process. In fact, adjusting the reaction temperature and not adding 12c4 for crystallization yielded a clean powder, which was identified by NMR spectroscopy as [Li][(Cp*Fe)(Cp'''Co)(μ,η^4:η^2:η^1-P_6CyH)].

While the starting material **1** is relatively stable, the obtained monoanionic compounds **2**–**5** are extremely sensitive towards air and especially moisture. Suitable crystals for single-crystal X-ray structure analysis were obtained by vapor diffusion of pentane in a dme solution (**2**, **3**) or by layering a dme solution with hexane (**4**) or pentane (**5**). The anions in **2** and **3** reveal a *catena*-P_5R ligand as middle deck in an envelope-type conformation (Figure 3).

The P_5R ligand coordinates in η^4 fashion to the {Cp*Fe} fragment via four P atoms in a nearly square planar P_4 unit (**2**) or in a distorted P_4 unit (**3**), respectively, similarly to the parent compound [Cp*Fe(η^4-P_5R)]$^-$.[7] However, the coordination to the {Cp'''Co} fragment differs. While in **2** the P atoms at the end of the P_5R chain and the P atom bearing the organic substituent coordinate to {Cp'''Co}, the P_5Me ligand (**3**), in contrast, coordinates via three adjacent P atoms (P1-P2-P3). Further, in **2**, the P1 atom bearing the *t*Bu substituent deviates from the η^4-P_4 plane by 92.9°. In **3**, the Me group is attached to P3 in the backbone of the P_5 ligand and P1 is bent out of the plane by

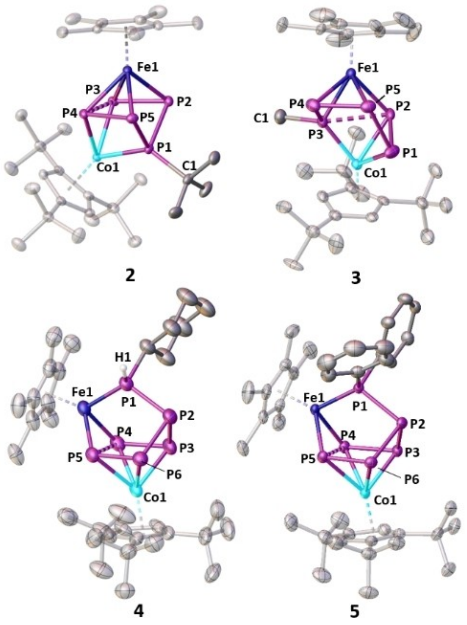

Figure 3. Molecular structures of the anions in **2**–**5** in the solid state; thermal ellipsoids are drawn at 50% probability level; H atoms attached to C atoms are omitted for clarity.

81.6° (for comparison in **1**: P1 is bent by 34°).[16] Contrary to **2** and **3**, in $[Cp^*Fe(\eta^4\text{-}P_5R)]^-$, the introduced substituent is always attached in endo position.[7]

The P3-P4 distance in **2** and the P2-P3 distance in **3** are considerably longer than a P–P single bond (**2**: 2.5466(4) Å; **3**: 2.6100(12) Å) and the WBIs of 0.63 (P3–P4, **2**) and 0.31 (P2-P3, **3**) indicate only P–P interactions. All other P–P bond lengths of the P_5R ligand in **2** and **3** are in the range of single bonds (**2**: P1–P2 2.1976(4), P1–P5 2.1832(4) Å; WBI in the range of 0.95 and 0.94; **3**: P3–P4 2.1565(11) Å, P1–P5 2.2324(11) Å; WBI in the range of 0.96–1.00) or formal double bonds (**2**: P2–P3 2.1729(5) Å, P4–P5 2.1644(5) Å, WBI in the range of 1.09; **3**: P4–P5 2.1331(14) Å, P1-P2 2.1821(13) Å, WBI in the range of 1.12–1.13). The twofold bridged P–P distances of P3–P4 (**2**) and P2–P3 (**3**) are highly elongated compared to the P–P single bonds in **1** (2.1459(10) - 2.2441(11) Å).[16] Hence the pnictogen ligands represent rather a *catena*-P_5R motif of the middle deck. The P–C bond lengths in **2** (1.8841(3) Å) and **3** (1.8534(4) Å) are in the range of single bonds and compare well to the P–C bond lengths in the similar complexes of the type $[(^{Mes}BIAN)Co(\eta^4\text{-}P_5R_2)]$ (1.8423(1)–1.897(3) Å, $(^{Mes}BIAN)$ = 1,2-bis(2,4,6-dimethylphenylimino)acenaphthene, R = *i*Pr, *t*Bu, Cy).[7,21–23]

In the solid state, $[Li(12c4)_2][(Cp^*Fe)(Cp'''Co)(\mu,\eta^4:\eta^2:\eta^1\text{-}P_6CyH)]$ (**4**) and $[K(2,2,2\text{-crypt})][(Cp^*Fe)(Cp'''Co)(\mu,\eta^4:\eta^2:\eta^1\text{-}P_6Ph_2)]$ (**5**) represent triple decker complexes with folded P_6RR' middle decks (Figure 3). In solid state compound **4** consists of two isostructural but independent anions within the asymmetric unit, which differ only slightly in their metrical parameters. Therefore, the crystallographic data for only one anion of **4** will be discussed (see Supporting Information). The PR_2 unit is attached to the P2 atom, which is bent out of the plane of the planar middle deck (P3-P4-P5-P6) by 114.2° (**4**) or 116.6° (**5**), respectively. The $P_6R'R''$ units reveal a P_5 ligand with an exocyclic {PR'R''} unit, which coordinates in η^1 fashion to the Fe atom together with one side of the P_5 unit in η^2 fashion. Four atoms of the P_6 core (P3–P4–P5–P6) coordinate in η^4 fashion to the Co atom. The Fe1-Co1 distance amounts to 3.8241(8) Å (**4**), and 3.7537(5) Å (**5**), respectively. The three Fe–P distances are 2.2118(11) Å, 2.2048(12) Å and 2.1305(10) Å (WBI in the range of 0.56-0.59) for compound **4** whereas the Fe1-P1 bond is shorter than the other distances. For **5**, the Fe–P lengths are in a similar range and thus in the range of Fe–P single bonds.[21] The P–P bond lengths of the phosphorus ligand in **4** are in the range of single bonds (P1–P2 2.2220(14), P2–P3 2.2115(14), P2–P6 2.2032(14) Å, WBI in the range of 0.81–0.98) or elongated double bonds (P3–P4 2.1589(14) Å, P5–P6 2.1637(13) Å, WBI of 1.11).[21,22] The P4–P5 distance amounts to 2.5450(13) Å and the corresponding WBI of 0.42 indicates P–P interactions. All P–P bonds in **5** are comparable with those in **4**, the bond lengths differ between single bonds (P1–P2 (WBI 0.88), P2–P3 (WBI 0.98), P2–P6 (WBI 0.98)) and double bonds (P3–P4 (WBI 1.12), P5–P6 (WBI 1.12). The P4–P5 distance amounts to 2.5880(7) Å (WBI of 0.39) and can only be considered as an interaction.

To elaborate the molecular structure of the obtained anionic complexes **2**–**5** in solution, they were investigated by multinuclear NMR spectroscopy in thf-d_8. Compound **2** shows a highly dynamic behavior in solution, which was studied by variable temperature NMR spectroscopy. At room temperature, the ^1H NMR spectrum reveals a doublet for the *t*Bu group ($^3J_{HP}$ = 9 Hz), three sharp singlets for the *t*Bu groups of the Cp''' ligand and the Me groups of the Cp* ligand. Further, a broad singlet for the C–H groups (Cp''') and two triplets ($^3J_{HH}$ = 5 Hz each) and a singlet for the 2,2,2-cryptand can be observed. The $^{31}P\{^1H\}$ NMR spectrum at room temperature shows three broad signals at δ = 30.3, −61.4 and −85.4 ppm with $\omega_{1/2}$ = 1600–2100 Hz. Upon cooling to −80 °C, in the ^1H NMR spectrum, the signal for the *t*Bu group changes to a sharp singlet and the broad signals for the *t*Bu groups of Cp''' sharpen as well as the triplets for the cryptand (Figure S1 and S3, Supporting Information). Further, the broad signals observed in the $^{31}P\{^1H\}$ NMR spectrum at room temperature split into five multiplets at −80 °C centered at δ = 33.4, −58.4, −86.7, −89.9 and −89.9 ppm with an integral ratio of 1:1:1:1:1 displaying an AMNOS spin system. The broadening of the signals for all *t*Bu groups and the signals for the cryptand molecules at room temperature indicate that the tumbling of the Cp''', the *t*Bu substituent and the counter-ion are responsible for the dynamic processes. In general, the $^{31}P\{^1H\}$ NMR spectra of **2**–**5** reveal sophisticated spin systems (AMNOS (**2**, **3**), AMNOSX (**4**) or ADD'MXX' (**5**)), which were iteratively fitted (cf. Supporting Information). In the ^{31}P NMR spectrum of **4**, the $^1J_{H\text{-}P}$ coupling of 250 Hz to the hydrogen atom directly attached to phosphorus can be detected as well as the $^2J_{H\text{-}P}$ (13 Hz) coupling to the neighboring P atom can be resolved in the ^1H NMR spectrum (cf. Supporting Information). The coupling of the hydrogen atoms of the substituents to the P_5/P_6 moiety is confirmed in the ^1H NMR spectra. For the *t*Bu group in **2** (δ = 0.66 ppm), a coupling constant of $^3J_{H\text{-}P}$ = 9 Hz is

observed, whereas the $^{2}J_{H\text{-}P}$ coupling cannot be resolved for the Me group in **3** ($\delta = 1.94$ ppm).

Upon functionalization of **1** by main group nucleophiles of group 14 and 15, the anionic triple-decker complexes **2–5** containing different chain-like P_5R and $P_6R'R''$ units were obtained. The nature of the obtained complexes is dependent from the nucleophile used. While carbon centered nucleophiles lead to the functionalization of the P_5 core and eventual distortion induced by the steric bulk of the nucleophile, the reaction with phosphorus centered nucleophiles lead to the extension of the P_5-unit, and in general, due to the presence of coordinatively active lone pair of the phosphorus atom (originating from the nucleophile) to additional coordination to the metal center, leading to more severe rearrangement of the P_n unit. Compounds **2–5** bear a negative charge, they might be prone to react with electrophiles, analogously to the parent complex **IX**, or can be chemically oxidized by Ag salts. The electrostatic potential surface of the complexes **2**, **4** and **5** (Figure 4) rather shows a localized negative charge on the polypnictogen middle decks, indicating that the electrophile would attack at that position as identified by the NBO analysis. The charge distribution for complex **2** provides the most positive values (0.01 and −0.02) for P3 and P4, whereas the charge values are much lower (−0.14 and −0.15) for P2 and P5. This suggests an electrophilic attack at P3 or P4. For complex **4** and **5**, the charge distribution is similar to that of **2** exhibiting the most positive values for P4 and P5 (**4**: −0.04 and −0.05; **5**: −0.04 and −0.05) in the backbone of the pnictogen ligand and the most negative values for P2, P3 and P6 (**4**: −0.17, −0.15 and −0.14; **5**: −0.14, −0.14 and −0.12). Therefore, the attack of an electrophile in **4** and **5** is expected to occur at the positions P4 or P5.

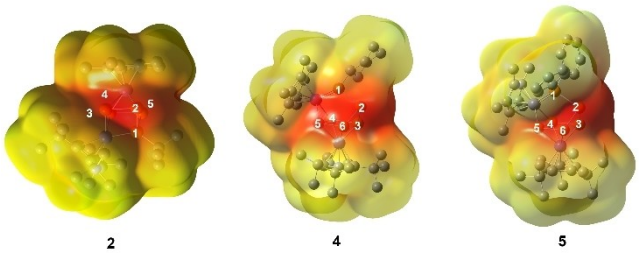

Figure 4. Electron potential mapped on electron density for **2**, **4** and **5**. Color code: blue = positive, red = negative (BP86-D3BJ/def2-TZVP level of theory).

Therefore, the reactivity of **2–5** towards MeI was studied (Scheme 3). The reaction of **2**, **4** and **5** with methyl iodide leads to the formation of 1,3 or 1,4 disubstituted $P_5R'\text{-}PR_2$ ligands in [(Cp*Fe)(Cp'''Co)(μ,η³:η²:η¹:η¹-P₅*t*BuMe)] (**6**), [(Cp*Fe)(Cp'''-Co)(μ,η⁴:η²:η¹-P₆CyHMe)] (**7**) and [(Cp*Fe)(Cp'''Co)(μ,η⁴:η²:η¹-P_6Ph_2Me)] (**8**). After workup, the complexes **6**, **7** and **8** were isolated in crystalline yields of 74%, 4% and 62%, respectively, and reveal unprecedented P_5R_2 and P_6R_3 organophosphorus ligands (Scheme 3, Figure 5). Complex **7** crystallizes in a rather low yield, although the ^{31}P NMR spectrum of the reaction solution shows a clean conversion. Even using isolated **4** for the quenching reaction with MeI did not improve the yield of

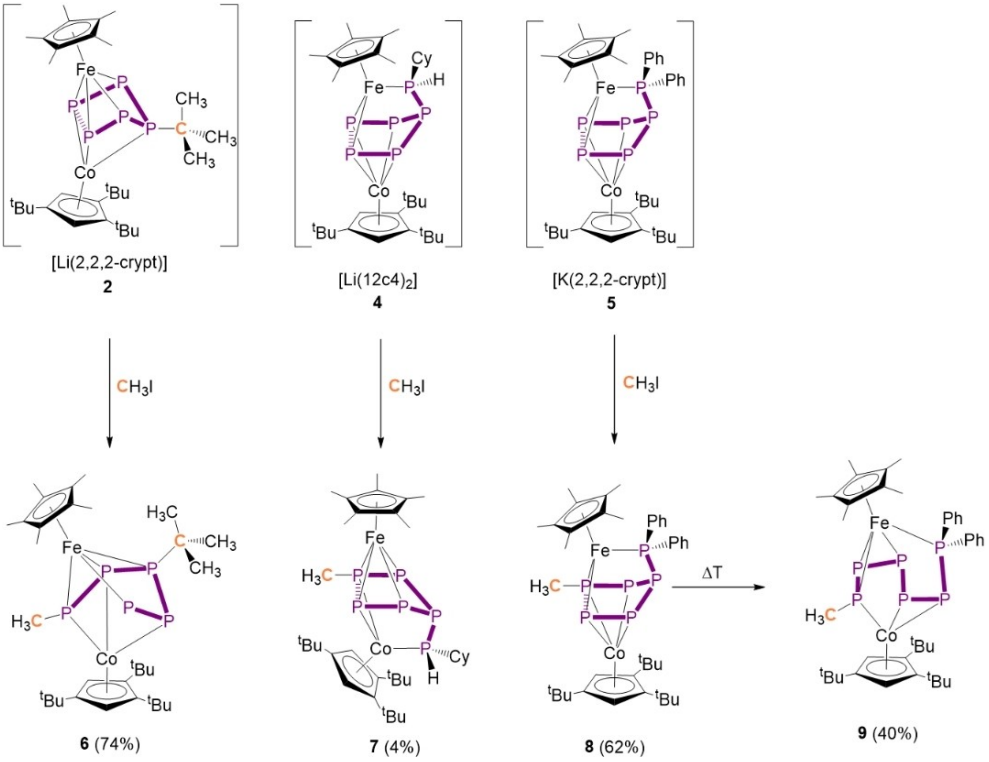

Scheme 3. Reactivity of **2**,**4**,**5** towards the carbon-based electrophile CH_3I; reactions were carried out in thf at rt (**6**) or −80 °C (**7**, **8**); thermal isomerization of **8** to **9** after 12 h at 110 °C. The yields in parentheses correspond to the isolated crystalline material (for further information see Supporting Information).

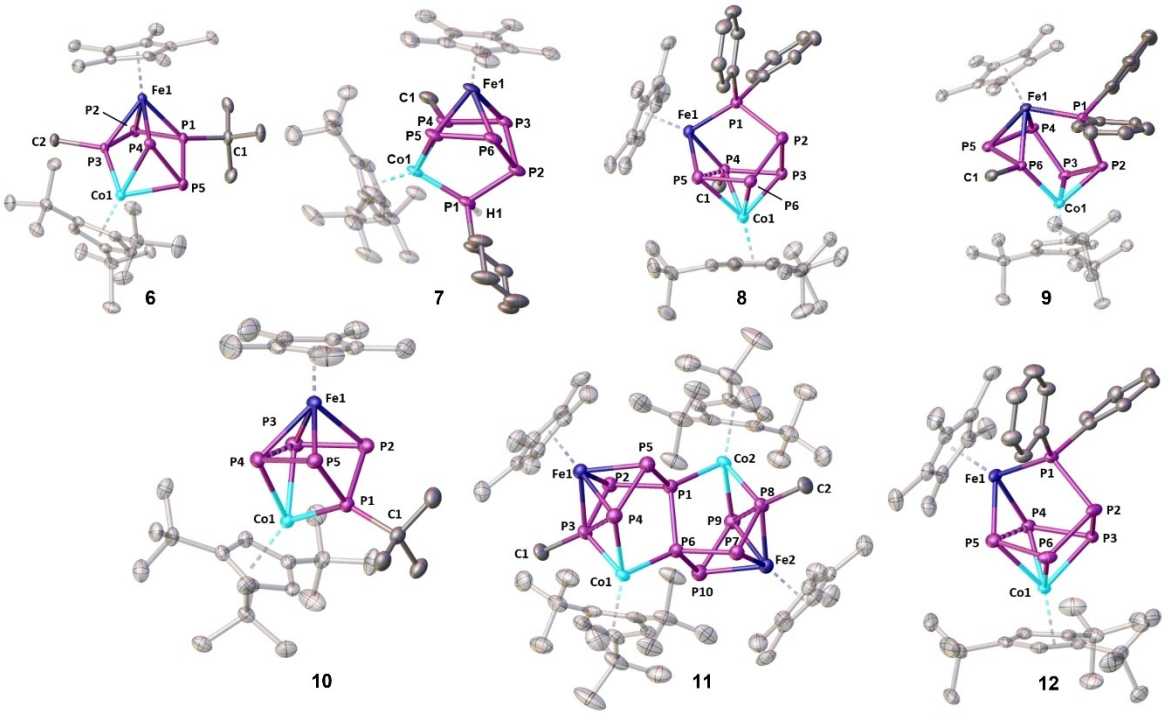

Figure 5. Molecular structures of complexes **6**–**12** in the solid state; thermal ellipsoids are drawn at 50% probability level; H atoms attached to C atoms are omitted for clarity.

isolated **7**. After crystallization, in the mother liquor still sets of signals for **7** and, interestingly, for **IX** can be detected. Probably, **7** decomposes over the time or some redox processes take place, which were observed for the formation of **4** as well. Interestingly, the reaction of **3** with MeI led to a selective but incomplete formation of [Cp*Fe(η^5-P_5)] independent of the reaction conditions. Apart from [Cp*Fe(η^5-P_5)], other sets of signals that could not be assigned were observed in the ^{31}P NMR spectrum. Thus, MeOTf was reacted with **3**. In this reaction, no formation of [Cp*Fe(η^5-P_5)] was observed and five signals with an integral ratio of 1:1:1:1:1 for a major product as well as some signal sets for minor products were observed in the reaction solution by ^{31}P NMR spectroscopy. The major product shows an AMNOS spin system, and the coupling constants would fit a *catena*-P_5RR′ chain. However, despite several attempts, the reaction mixture could not be purified by crystallization or column chromatography due to decomposition of the products (cf. Supporting Information).

In the solid state, the structures of the neutral organophosphorus complexes **6**, **7** and **8** reveal each bent triple-decker geometry containing versatile middle decks. In **6**, the two organic groups are in a 1,3 position of the *catena*-P_5R_2 ligand which coordinates in η^3:η^1 fashion to {Cp*Fe} and in η^2:η^1 fashion to {Cp‴Co}, respectively. Also, in **7** and **8**, a 1,3-substitution pattern of the former P_5 unit in **1** is observed. Surprisingly, the methylation of **4** and **5** did not yield isostructural complexes. While in **7** the phosphorus atom of the CyHP group coordinates to the Co atom, in **8**, the phosphorus atom of the Ph_2P group coordinates to the Fe atom. This is presumably due to the different steric demands of the phosphanide residues.

Electrophilic quenching of [Cp*Fe(η^4-P_5R)]$^-$ leads to 1,1 substituted complexes of the type [Cp*Fe(η^4-P_5RR′)]$^-$ where the functionalized P atom is out of the η^4-P_4 plane with non-coordinating disubstituted structural P_5RR′ motifs,[7] whereas electrophilic quenching of **2** does not occur at P1 due to the inaccessibility of this lone pair, but takes place in the backbone at P3. The reaction of **2** with MeI leads selectively to the formation of the 1,3-substitution product **6**, which seems to be the most favored reaction product. In the ^{31}P NMR spectrum of the reaction solution of **6**, the formation of other isomers could not be detected.

Complexes **6**–**8** were characterized in solution by ^{31}P NMR spectroscopy in CD_2Cl_2 (**6**) and C_6D_6 (**7**, **8**) revealing complex AMNOS (**6**) and AMNOSX (**7**, **8**) spin systems, which were iteratively fitted (see Supporting Information). In the corresponding coupled ^{31}P NMR spectra, due to $^nJ_{P\text{-}H}$ (n = 2–3) coupling, a broadening of the signals corresponding to the PR_2 units in **6** and **8** can be observed. In **7**, due the coupling of the hydrogen atom directly bound to the phosphorus atom of the CyHP unit, the corresponding signal splits into a doublet of doublets ($^1J_{P\text{-}H}$ = 305 Hz) (see Supporting Information). In the ^{1}H NMR spectra of all compounds, the coupling of the hydrogen atoms of the organic substituents attached to phosphorus can be detected (**6**: $^2J_{H\text{-}P}$ = 8 Hz (Me), $^3J_{H\text{-}P}$ = 15 Hz (*t*Bu); **7**: $^1J_{H\text{-}P}$ = 305 Hz (H), $^2J_{H\text{-}P}$ = 8 Hz (Me); **8**: $^3J_{H\text{-}P}$ = 7 Hz (Me)).

Heating a toluene solution of **8** to 110 °C for 12 h leads to [(Cp*Fe)(Cp‴Co)(μ,η^3:η^2:η^1:η^1-P_6Ph_2Me)] (**9**), which can be iso-

lated in 40% crystalline yield (Scheme 3). Upon heating a solution of **8**, the formation of two new sets of signals can be observed in the ^{31}P NMR spectrum and the signals for **8** partly remain. One new set of signals can be assigned to compound **9**, which could be isolated, whereas the second set of signals can be assigned to an insertion product of the {PPh_2} group to a *cyclo*-P_6Ph_2Me ligand, but this compound (**9′**) could not be crystallized regardless of several attempts (see Supporting Information). After 1 h of heating, the two new compounds with an integral ratio of the three compounds of 1.2:1.0:1.3 (**9**:**8**:**9′**) could already be detected. After 12 h, a ratio of 10.6:1.0:4.8 is present and does not change any more. After column chromatographic workup, **9** could be crystallized. In the solid state, **9** exhibits a *catena*-P_6Ph_2Me middle deck, which is formed by rearrangement processes, probably by migration of the Ph_2P or Me groups. The *catena*-P_6Ph_2Me ligand coordinates in $\eta^3{:}\eta^1$ fashion to {Cp*Fe} and in $\eta^2{:}\eta^1$ fashion to {Cp‴Co} (Scheme 3; for further details see Supporting Information). A possible thermally induced rearrangement of **7** could not be investigated so far due to its low crystalline yield. Heating a toluene solution of **6** to 110 °C for 1 h exhibited only a slight decomposition to [Cp*Fe(η^5-P_5)] (**IX**) in the ^{31}P NMR spectrum and did not provide any new sets of signals. After heating the sample to 110 °C for 6 h, the ratio of **IX**:**6** increased to 0.62:1.00 and, after 12 h, the ratio changed slightly to 0.64:1.00 (see Supporting Information).

Since the complexes **2–5** are anionic, it is to be expected that they are prone to oxidation. The chemical oxidation of **2**, **3** and **5** with $AgBF_4$ in thf affords the paramagnetic complexes [(Cp*Fe)(Cp‴Co)(μ,$\eta^4{:}\eta^2{:}\eta^1$-P_5tBu)] (**10**) and [(Cp*Fe)(Cp‴-Co)(μ,$\eta^4{:}\eta^2{:}\eta^1$-P_6Ph_2)] (**12**) as well as the diamagnetic complex [$(Cp^*Fe)_2(Cp'''Co)_2(\mu_4,\eta^4{:}\eta^4{:}\eta^2{:}\eta^2{:}\eta^1{:}\eta^1$-$P_{10}Me_2$)] (**11**) (Scheme 4). Complexes **10** and **12** could be isolated in 30% and 62% crystalline yield, respectively. According to ^{31}P NMR spectroscopy, **3** reacts to **11** upon oxidation although the reaction is not selective (see Supporting Information). A clean reaction was achieved by reacting [Cp*Fe(η^4-P_5Me)]$^-$ with 0.5 equiv. of {Cp‴CoCl}$_2$ in thf (crystalline yield of **11**: 78%). Regardless of numerous attempts, the oxidation of **4** with $AgBF_4$ to an analogous complex of the formulae [(Cp*Fe)(Cp‴Co)(P_5R)] (R = PCyH) has so far not been even possible. Upon oxidation of **4** with $AgBF_4$, the protonated complex [(Cp*Fe)(Cp‴-Co)(μ,$\eta^3{:}\eta^2{:}\eta^1$-P_6CyH_2)] featuring a *catena*-PH-P_4-PCyH chain and the redox product $(CyP)_4$ were isolated. These products were obtained independent of the reaction conditions and the choice of solvent (thf or *o*-difluorobenzene) and silver salt ($AgBF_4$ or AgTEF) used.

DFT calculations show that the different behaviors of **2**, **3** and **5** upon oxidation are due to the spin density distribution in the oxidized species. In [(Cp*Fe)(Cp‴Co)(μ,$\eta^4{:}\eta^2{:}\eta^1$-P_5Me)] (one half of complex **11**), the spin density is located at the Fe and Co atoms but also at the phosphorus atom next to the substituted P atom (Figure 6). In **10** and **12**, the spin density is also mainly located on the metal atoms but, in **12**, no spin density is located on the P atoms. In **10**, also a contribution of the P atoms is present, but the dimerization is probably prevented due to steric hindrance (Figure 7).

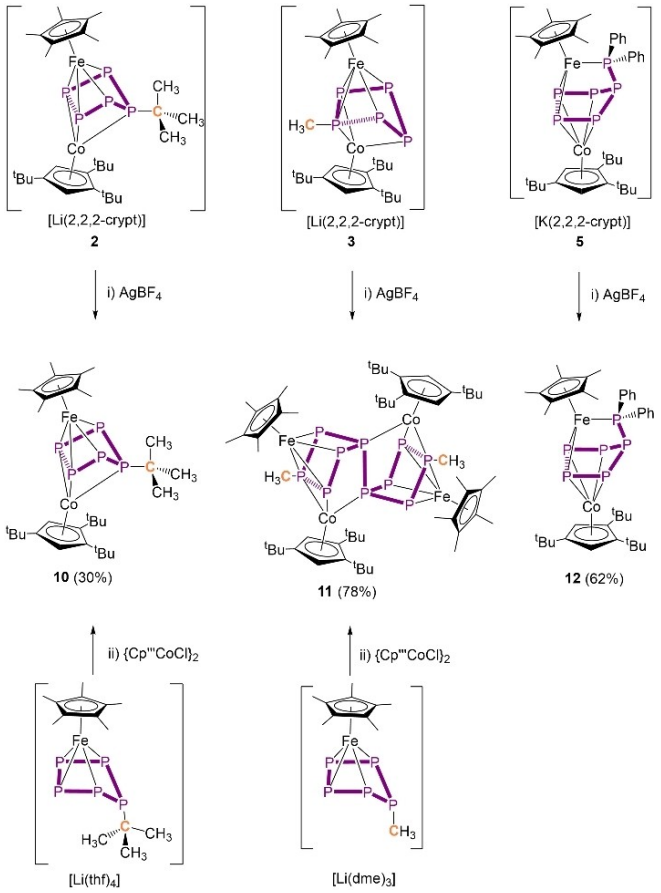

Scheme 4. Oxidation of **2**, **3** and **5** by $AgBF_4$ (i) and alternative procedures for the synthesis of **10** and **11** starting from [Cp*Fe(η^4-P_5R)]$^-$ (ii); in thf at room temperature; the yields provided in parentheses are for the isolated crystalline yields.

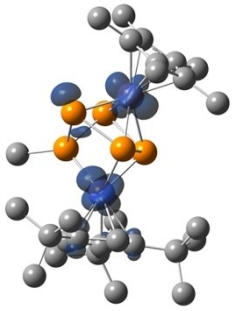

Figure 6. Iso-surfaces of the spin density in [(Cp*Fe)(Cp‴Co)(μ,$\eta^4{:}\eta^2{:}\eta^1$-P_5Me)]. Hydrogen atoms are omitted for clarity.

Upon the oxidation of **2–5**, the P_5tBu (**10**) and P_6Ph_2 (**12**) organophosphorus ligands do not undergo significant structural changes as for instance P–P bond formation or cleavage according to X-ray single-crystal structure analysis (Figure 5). Compound **10** is disordered in solid state over two positions. Therefore, just the major part will be discussed. However, the P3–P4 (**10**, **11**) or P4–P5 (**12**) distances become slightly shorter (**2**: 2.5466(4) Å; **10**: 2.3403(9) Å; **5**: 2.5880(7) Å; **12**: 2.3935(7) Å).

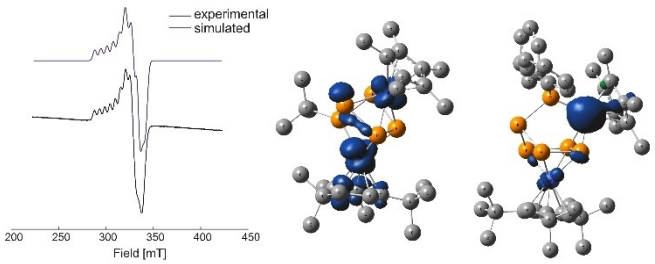

Figure 7. Experimental (black) and simulated (blue) X-band EPR spectra of **10** in frozen toluene solution (left) and the iso-surfaces of the spin density in **10** (middle) and **12** (right). Hydrogen atoms were omitted for clarity.

In **10**, the P–P bond lengths are in the range of short single bonds (P1–P2, P2–P3, P4–P5, P5–P1 2.1706(8) to 2.1894(8) Å, the WBIs in the range of 0.96 to 1.07). In **12**, the P1–P2, P2–P3 and P2–P6 distances are slightly longer (WBI 0.86–0.97) than the P3–P4, P5–P6 distances (WBI 1.03 and 1.07). The P atom bearing the organic substituent in **10** and **11** deviates from the P_4 plane defined by the other four P atoms by 79.2° and 62.5°, respectively.

The structure of **11** in the solid state exhibits a dimeric complex containing an unprecedented $P_{10}Me_2$ ligand that can be best described as two η^4-P_5Me units in envelope conformation linked via a P–P single bond (P1–P6 2.190(2) Å, WBI 0.84). The $P_{10}R_2$ bridging ligand displays an open-edged dihydrofulvalene analog in the tetranuclear cluster. Each P_5Me unit of the ligand coordinates in η^4 fashion to one {Cp*Fe} fragment and in $\eta^2{:}\eta^1$ fashion to one {Cp'''Co} fragment. The other P–P bond lengths are slightly longer and in the range of single bonds (P1–P2, P2–P5; WBI 0.84 and 0.89) or elongated double bonds (P2–P3, P4–P5; WBI 1.04 and 1.14), showing P–P bond alternation. The Co–P distances are in the range of 2.177(2) Å to 2.333(6) Å and Fe–P distances in the range of 2.2359(14) to 2.3624(14) Å. As the Co atoms are slightly disordered just the major part was discussed.

To date, a number of charged and neutral complexes are known that feature a similar bridging P_{10} ligand as in **11**, that is, $[\{(C_5H_3(SiMe_3)_2Co\}_4P_{10}]$[24] (**XIV**) and $[\{(C_5H_3(t\text{Bu}))Rh\}_2(P_5\text{-}P_5)(Rh(C_5H_3(t\text{Bu})_2)\}]$[25] (**XV**), but, to the best of our knowledge, none of them contains a P_{10} ligand functionalized with organic groups. Therefore, by one electron oxidation of **3** or electrophilic quenching of $[Cp^*Fe(\eta^4\text{-}P_5Me)]^-$, respectively, the unique formation of an organo-functionalized $P_{10}Me_2$ ligand is possible.

Similar to **11**, peculiar neutral Rh- and Co-containing P_{10} species also reveal pronounced P–P bond alternation within the P_5 envelope-type units and an open-ring structure, which is suggested by the rather long P3-P4 distances (2.474(2) Å for **XIV**[24] and 2.624(2) Å for **XV**;[25] **11**: 2.5689(17) Å). In comparison, the charged complexes $[K(dme)K(dme)_2][(Cp^*Fe)_2(\mu,\eta^4{:}\eta^4\text{-}P_{10})]$ and $[(Cp^*Fe)_2(\mu,\eta^4{:}\eta^4\text{-}P_{10})][SbF_6]_2$ feature closed-ring structural motifs, but the single bond connecting both P_5 envelopes is in the same range as for **11** (2.119(1) Å (P_{10}^{2-}), 2.190(2) Å (**11**)).[26]

Complex **11** was characterized in solution by multinuclear NMR spectroscopy, **10** and **12** by X-band EPR spectroscopy. The $^{31}P\{^1H\}$ NMR spectrum of **11** at room temperature displays broad signals indicating a dynamic behavior in solution, presumably due to the hindered rotation of the Cp''' ligands. Cooling to −60 °C leads to well-resolved signals of a high order spin system (AA'MM'NN'SS'XX') containing five multiplets centered at δ = 232.6, 35.6, 26.2, −134.7 and −223.7 ppm with an integral ratio of 2:2:2:2:2, which was iteratively fitted (see Supporting Information).

Both the silent ^{31}P NMR and the active X-band EPR spectra of **10** and **12** suggest paramagnetic complexes. For **10**, in the ^1H NMR spectrum, broad and shifted signals can be assigned to the hydrogen atoms of the Cp^R ligands and organo-substituents. The X-band EPR spectra of both compounds in toluene solution at −80 °C reveal strong rhombic signals with *g* values near to 2 indicating the presence of one unpaired electron (**10**: $g_1 = 2.196$, $g_2 = 2.075$, $g_3 = 1.995$; **12**: $g_1 = 2.3892$, $g_2 = 2.1029$, $g_3 = 2.15236$). Further, the EPR spectrum of **10** exhibits a well-resolved hyperfine coupling to cobalt ($A_1^{Co} = 190.8$, $A_2^{Co} = 35.3$, $A_3^{Co} = 23.9$ MHz). In comparison, the EPR spectrum of **12** is more asymmetric containing more distinct *g* values (see Supporting Information). The effective magnetic moments were determined to be 1.77 μ_B (**10**) and 1.36 μ_B (**12**) by the Evans NMR method corresponding to about one unpaired electron each. DFT calculations reveal that the spin density in **10** is located at the Fe and Co atoms with minor contribution of the P atoms (Figure 7). In complex **12**, the spin density is strongly located on the Fe1 atom, which is in agreement with the absence of hyperfine coupling to Co (cf. Supporting Information). In both cases no P–P bond formation was observed. In the EPR spectrum of **10** hyperfine coupling to the Co nucleus is detected, showing that the spin density is *inter alia* located at the Co atom, which is in agreement with the results of DFT calculations (Figure 7). This indicates that the oxidation occurs at the Co center. For **10** and **12** no hyperfine coupling to the phosphorus atoms can be detected in the EPR spectrum, thus we assume metal centered oxidation processes. The electronic structure of both complexes is in accordance with the results of the DFT calculations.

Reactivity studies of **12** and **10** show that a further oxidation by one equivalent of Ag[FAl] ([FAl] = $[FAl\{OC_6F_{10}(C_6F_5)\}_3]$) yields the cationic complexes $[(Cp^*Fe)(Cp'''Co)(\mu,\eta^3{:}\eta^2{:}\eta^2{:}\eta^1\text{-}P_6Ph_2)][FAl]$ (**13**) and $[(Cp^*Fe)(Cp'''Co)(\mu,\eta^5{:}\eta^4\text{-}P_5t\text{Bu})][FAl]$ (**14**) in 53 % yield and 39 % yield, respectively (Scheme 5).

Upon oxidation of **12**, the rearrangement of the P_6Ph_2 ligand was observed leading to the formation of a 1,1-diphenyl hexaphosphane middle deck in **13**. The P_6Ph_2 ligand coordinates to the Fe atom in $\eta^3{:}\eta^1$ fashion and to the Co atom in η^4 fashion (Figure 8). Upon rearrangement, the bond cleavage of one P–P bond was observed. For complex **10**, a formal isomerization of the middle deck was observed upon oxidation to **14**. The molecular structure in the solid state of the cationic part in **14** shows a slightly bent triple decker complex built up by an envelope-type P_5tBu middle deck, which is η^5-coordinating to {Cp*Fe} and η^4-coordinating to {Cp'''Co} (Figure 8). The middle deck in **14** displays a rare substitution pattern as the *t*Bu substituent is not attached to the out-of-plane P atom. For the P_5tBu middle deck, P–P bond formation upon oxidation can be observed as the P3–P4 distance becomes shorter compared to

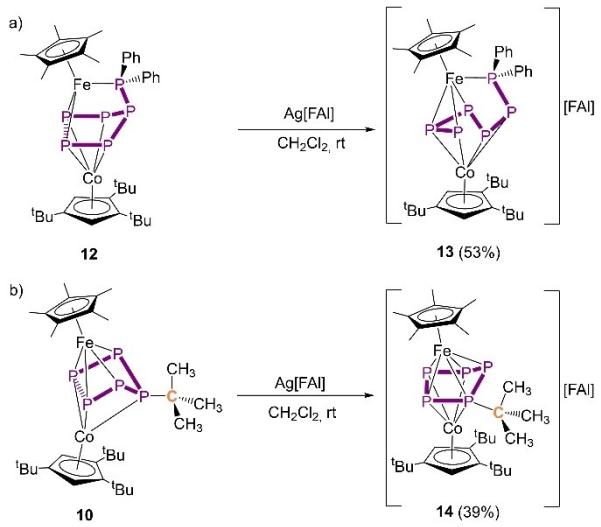

Scheme 5. a) Reactivity of **12** towards Ag[FAl] in CH_2Cl_2; b) reactivity of **10** towards Ag[FAl] in CH_2Cl_2; the yields provided in parentheses are for the isolated crystalline yield.

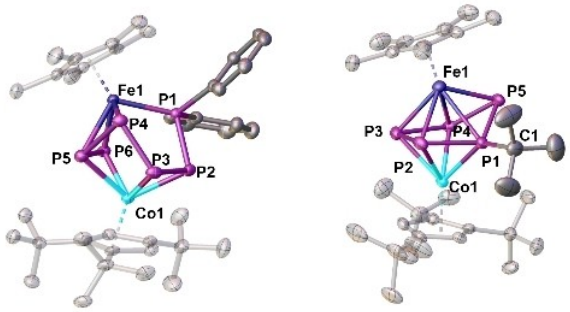

Figure 8. Molecular structures of the cations in **13** (left) and **14** (right) in the solid state; thermal ellipsoids are drawn at 50% probability level; H atoms are omitted for clarity.

10 in the solid state (**10**: P3–P4 2.3403(9) Å; **14**: P3–P4 2.2779(12) Å, WBI of 0.76) and can be considered as an elongated single bond. All other P–P distances are in the range of single bonds (P1–P2 2.2585(12), WBI of 0.73; P3–P4; P4–P5 2.1857(13), WBI of 0.96) or double bonds (P2–P3 2.1115(13), WBI of 1.15; P5–P1 2.1059(12), WBI of 1.05) and compare well to the ones in **1**. Overall, the twofold oxidation of the anionic complex **2** to the neutral species **10** and further to the cationic complex **14** emphasizes the high stability and versatility of the P_5*t*Bu middle deck in particular. This reactivity behavior displays a rare example of the oxidation chemistry of P_nR^- ligands in the coordination sphere of transition metals.

Due to its sensitivity, complex **13** could not be fully characterized and decomposition products were observed in the ^{1}H NMR spectrum already when dissolving crystalline samples of **13**. [(Cp*Fe)(Cp'''Co)(μ,η^5:η^5-P_5)][FAl] was identified by X-band EPR spectroscopy to be one of the decomposition products.[27] Nonetheless, the molecular ion peak in the ESI mass spectrum at *m/z* = 823.1 (100%, $[M]^+$) and the elemental analysis go with **13**.

In solution, the cation of **14** shows dynamic behavior studied by multinuclear variable temperature NMR spectroscopy. At room temperature, only one broad triplet at δ = −45.2 ppm can be observed in the $^{31}P\{^1H\}$ NMR spectrum in CD_2Cl_2 which could be assigned to the P1 atom bearing the organic substituent. The ^{1}H NMR spectrum reveals a doublet for the *t*Bu group ($^3J_{H\text{-}P}$ = 20 Hz) and five singlets for the protons of the Cp''' and Cp* ligands. Upon cooling to −80 °C, in the ^{1}H NMR spectrum, the signal for the *t*Bu group broadens and is superimposed by the signal for the *t*Bu group of Cp''' ligand. Further, in the $^{31}P\{^1H\}$ NMR spectrum at −80 °C, five multiplets can be observed, centered at δ = 144.6, −45.2, −67.1, −204.8 and −308.3 ppm with an integral ratio of 1:1:1:1:1 displaying an AMNSX spin system that was iteratively fitted (see Supporting Information). Furthermore, **14** seems to be more stable than **13**, as, in solution, no decomposition products could be observed and only a molecular ion peak at m/z = 695.41 could be detected in the ESI mass spectrum.

Conclusions

In summary, we demonstrated the versatile functionalization of [(Cp*Fe)(Cp'''Co)(μ,η^5:η^4-P_5)] (**1**) via a sequence of nucleophilic-electrophilic or nucleophilic-oxidation reactions giving products in good to excellent yields. In the reaction of **1** with carbon-centered anionic nucleophiles, P–P bond cleavage is observed yielding P_5R middle decks (**2**, **3**). Utilizing phosphorus-centered nucleophiles, P_6R_2 middle decks containing an open-edged P_5 ligand with an exocyclic {PR_2} unit are formed. Subsequent electrophilic quenching revealed unique P_5R_2 (**6**) and P_6R_3 (**7**, **8**) organophosphorus ligand complexes in an unprecedented 1,3 (**6**) or 1,4 (**7**, **8**) substitution pattern. The overall twofold functionalization of **1** smoothly yields novel mononuclear di-organophosphorus complexes in contrast to the already known 1,1 substitution patterns of [Cp*Fe(η^4-P_5R_2)]. Beyond that, the approach of using the bimetallic complex **1** to stabilize PR_2^- nucleophiles at a former *cyclo*-P_5 unit turned out to be possible. Further, the oxidation of **2** and **5** results in the paramagnetic complexes $[(Cp^*Fe)(Cp'''Co)(P_5R)]^{\cdot}$ (**10**, **12**). In contrast, **4** dimerizes upon oxidation to form **11**, which contains a novel open-edged dihydrofulvalene-type $P_{10}R_2$ ligand. Since the formation of P-rich polyphosphorus complexes is an ongoing research topic, the presented sequence of transformations opens the way to P-rich multiple organo-substituted ligands. This approach emphasizes the versatility of the functionalization via the sequence of nucleophilic-electrophilic reactions. Moreover, the oxidations of **5** to **12** and then to **13** and of **2** to **10** and then to **14** show the high variability of the used triple decker system for chemical modifications via substitution and oxidation and these promising results pave the way for further investigations. Finally, this behavior emphasizes especially the high versatility of the P_5 middle deck in the heterobimetallic complex **1** and hence results in complexes with organo-

phosphorus substituents attached to the polypnictogen middle deck.

Experimental Section

General: All manipulations were performed using dry nitrogen standard Schlenk techniques or an argon filled glove box. Solvents were dried, degassed and distilled by using standard procedures. The compounds [(Cp*Fe)(Cp'''Co)(μ,η^5:η^4-P$_5$)] (**1**),[16] [Cp*Fe(η^5-P$_5$)] (**IX**),[28] [{Cp'''CoCl}$_2$][29] and Ag[FAl][30] were synthesized according to literature known procedures. $KPPh_2$ was synthesized from KH and PPh_2H in dme. $LiPPh_2$ and LiPCyH were synthesized from PPh_2H or $CyPH_2$, respectively, and ^{n}BuLi in hexane. *t*BuLi, EtLi, *sec*BuLi (Lithium butan-2-ide), MeLi, MeI, $AgBF_4$, 2,2,2-cryptand and 12c4 were commercially available. NMR spectra were recorded on a Bruker Avance 400 (^{1}H: 400.132 MHz, ^{19}F: 376.498 MHz, ^{31}P: 161.975 MHz) or 300 (^{1}H: 300.131 MHz) spectrometer. Chemical shifts are referenced to $SiMe_4$ (^{1}H NMR), $CFCl_3$ (^{19}F NMR) and 85 % H_3PO_4 (^{31}P NMR) as external standard. Chemical shifts are given in ppm and coupling constants J in Hertz [Hz] without considering their sign. ESI mass spectra were recorded using a ThermoQuest Finnigan TSQ 7000 spectrometer. LIFDI mass spectra were recorded using a Finnigan MAT 95 mass spectrometer. Data for elemental analysis is accomplished by a Vario EL III apparatus. The X-band EPR measurements were performed with a MiniScope MS400 device with a frequency of 9.44 GHz and a rectangular resonator TE102 of the company Magnettech GmbH.

Synthesis of 2: A solution of [(Cp*Fe)(Cp'''Co)(μ,η^5:η^4-P$_5$)] (100 mg, 0.1567 mmol, 1 equiv.) in thf was cooled to −80 °C and a *t*BuLi solution in pentane (0.63 mL, 0.249 mol/L, 0.1567 mmol, 1 equiv.) was added, while the color changed slightly from violet to red-brown. After five minutes a solution of 2,2,2-cryptand (59 mg, 0.1567 mmol, 1 equiv.) in thf was added and the mixture then warmed to room temperature. The solvent was removed under vacuum and the residue washed with hexane (weakly red colored). The residue was dissolved in dme and crystals were obtained by slow vapor diffusion of pentane in the dme solution. By this way, single crystals of [Li(2,2,2-crypt)][(Cp*Fe)(Cp'''Co)(μ,η^4:η^2:η^1-P$_5$*t*Bu)], [Li(2,2,2-crypt)][(Cp*Fe)(Cp'''Co)(μ,η^4:η^3-P$_5$)] and [Li(opened-2,2,2-crypt)][(Cp*Fe)(Cp'''Co)(μ,η^4:η^2:η^1-P$_5$*t*Bu)] were obtained. After sorting under the microscope, [Li(2,2,2-crypt)][(Cp*Fe)(Cp'''Co)(μ,η^4:η^3-P$_5$*t*Bu)] (**2**) could be isolated as large brown blocks. The supernatant was decanted off, the obtained crystals washed with hexane and dried under vacuum. Yield (**2**): 43 mg (26 %).

Synthesis of 3: A solution of [(Cp*Fe)(Cp'''Co)(μ,η^5:η^4-P$_5$)] (200 mg, 0.3133 mmol, 1 equiv.) in thf was cooled to −80 °C and a MeLi solution in Et_2O (0.39 mL, 0.802 mol/L, 0.3133 mmol, 1 equiv.) was added, while the color changed slightly from violet to red-brown. After five minutes a solution of 2,2,2-cryptand (118 mg, 0.3133 mmol, 1 equiv.) in thf was added and then the mixture was warmed to room temperature. The solvent was removed under vacuum. The residue was dissolved in dme and crystals of [Li(2,2,2-crypt)][(Cp*Fe)(Cp'''Co)(μ,η^4:η^2:η^1-P$_5$Me)] (**3**) were obtained by slow vapor diffusion of pentane in the dme solution. The supernatant was decanted off, the obtained crystals washed with hexane and dried under vacuum. Yield (**3**): 252 mg (76 %).

Synthesis of 4: a) A solution of LiPCyH (95.5 mg, 0.783 mmol, 1 equiv.) in thf was added to a stirred solution of [(Cp*Fe)(Cp'''-Co)(μ,η^5:η^4-P$_5$)] (500 mg, 0.783 mmol, 1 equiv.) in thf at −80 °C, while the color changed immediately from red to red-brown. After stirring for 5 min, 12c4 (11.6 mL, 1.566 mmol, 0.135 mol/L in dme, 2 equiv.) was added and warmed to room temperature. Within two hours, the color changed to green. The solvent was removed under vacuum. The green oily residue was dissolved in a small amount of thf and precipitated by addition of an excess of pentane. The supernatant was decanted off and dried under vacuum. [Li-(12c4)$_2$][(Cp*Fe)(Cp'''Co)(μ,η^4:η^2:η^1 -P$_6$CyH)] (**4**) was isolated as dark green powder. Very few single crystals could be obtained from a concentrated solution in dme layered with hexane at −30 °C. In the phosphorus and hydrogen NMR spectra of the green powder always impurities were observed. Therefore, an alternative procedure was applied. Yield (**4**): 507 mg (58 %). b) A solution of LiPCyH (38.3 mg, 0.313 mmol, 1 equiv.) in thf was added to a stirred solution of [(Cp*Fe)(Cp'''Co)(μ,η^5:η^4-P$_5$)] (200 mg, 0.313 mmol, 1 equiv.) in thf at room temperature, while the color changed immediately from red to green. After stirring for 15 min the solvent was removed under vacuum, the residue washed with pentane. After drying under vacuum [Li][(Cp*Fe)(Cp'''Co)(μ,η^2:η^1:η^4-P$_6$CyH)] can be isolated as dark green powder. Yield: 135 mg (41 %).

Synthesis of 5: A solution of $KPPh_2$ in dme (2.77 mL, 0.113 mol/L, 0.313 mmol, 1 equiv.) was added to a stirred solution of [(Cp*Fe)(Cp'''Co)(μ,η^5:η^4-P$_5$)] (200 mg, 0.313 mmol, 1 equiv.) and 2,2,2-cryptand (118 mg, 0.313 mmol, 1 equiv.) in thf at −80 °C. The color changed from dark red to brown. The reaction mixture was warmed to room temperature, while the color changed to green. The solvent was reduced, layered with pentane, and stored at −30 °C. After a few days, [K(2,2,2-crypt)][(Cp*Fe)(Cp'''Co)(μ,η^4:η^2:η^1-P$_6$Ph$_2$)] (**5**) crystallizes as dark green blocks. The supernatant was decanted off, the crystals washed with hexane and dried under vacuum. Yield (**5**): 354 mg (91 %).

Synthesis of 6: A solution of [(Cp*Fe)(Cp'''Co)(μ,η^4:η^3-P$_5$)] (500 mg, 0.783 mmol, 1 equiv.) in thf was cooled to −80 °C and *t*BuLi (0.76 mL, 0.783 mmol, 1.028 mol/L in pentane, 1 equiv.) was added, while the color changed immediately to red-brown. The reaction was warmed to room temperature and MeI (3 mL, 0.90 mmol, 0.30 mol/L in dme, 1.15 equiv.) was added. After stirring overnight, the solvent was removed under vacuum and the red-brown residue extracted with pentane. After filtration through diatomaceous earth, the solvent was removed under vacuum, the residue dissolved in CH_2Cl_2 and layered with acetonitrile. After a few days [(Cp*Fe)(Cp'''Co)(μ,η^3:η^2:η^2:η^1-P$_5$*t*BuMe)] (**6**) was obtained in form of dark brown blocks. The supernatant was decanted off and the crystals dried under vacuum. Yield (**6**): 411 mg (74 %).

Synthesis of 7: A solution of [(Cp*Fe)(Cp'''Co)(μ,η^5:η^4-P$_5$)] (400 mg, 0.626 mmol, 1 equiv.) in thf was cooled to -80 °C and a solution of LiPCyH (76.5 mg, 0.626 mmol, 1 equiv.) in thf was added. The reaction was warmed to room temperature, while the color changed from purple to green. After stirring for 2 h the reaction was cooled to −80 °C and MeI (0.39 mL, 0.626 mmol, 1.6 mol/L in dme, 1 equiv.) was added.[31] The reaction was warmed to room temperature and stirred for 2 h. Then the solvent was removed under vacuum, the residue extracted with toluene and filtered over diatomaceous earth. The solvent was removed under vacuum and the residue dissolved in Et_2O and transferred into a double Schlenk with a small amount of toluene on the second side. (Alternative procedure: The residue was dissolved in CH_2Cl_2 and layered with CH_3CN and stored at −30 °C). After a few days after storage at room temperature, [(Cp*Fe)(Cp'''Co)(μ,η^4:η^2:η^1-P$_6$CyHMe)] (**7**) could be isolated in form of dark blocks. The supernatant was decanted off and the crystals dried under vacuum. Yield (**7**): 20 mg (4 %).

Synthesis of 8: A solution of MeI in dme (0.177 mL, 0.161 mmol, 0.914 mol/L, 1 equiv.) was added to a stirred solution of [K(2,2,2-crypt)][(Cp*Fe)(Cp'''Co)(μ,η^2:η^1:η^4-P$_6$Ph$_2$)] (200 mg, 0.161 mmol, 1 equiv.) in thf at −80 °C. The color changed from brownish green to dark green. The reaction mixture was warmed to room temperature. Then the solvent was removed under vacuum. The residue was extracted with hexane, filtered over diatomaceous earth and

the solvent removed under vacuum. The residue was dissolved in CH_2Cl_2, layered with acetonitrile, and stored at −30 °C. After a few days, [(Cp*Fe)(Cp'''Co)(μ,η²:η¹:η⁴-P_6Ph_2Me)] (**8**) crystallizes as dark green rods. The supernatant was decanted off and the crystals dried under vacuum. Yield (**8**): 84 mg (62%).

Synthesis of 9: A solution of [(Cp*Fe)(Cp'''Co)(μ,η²:η¹:η⁴-P_6Ph_2Me)] (100 mg, 0.12 mmol) in toluene-d_8 was heated for 11.5 h (^{31}P NMR control) at 110 °C, while the color changed from dark green to brown. The solvent was removed under vacuum. The residue was dissolved in hexane, silica gel was added, and the solvent removed under vacuum. The preabsorbed mixture was purified by column chromatographic workup (SiO_2, hexane, 12×2 cm). With a mixture of hexane/toluene (7:3) a brown fraction was eluted. With a 1:1 mixture of hexane/toluene a reddish-brown fraction of [(Cp*Fe)(Cp'''Co)(μ,η³:η²:η¹:η¹-P_6Ph_2Me)] (**9**) was eluted. After removing the solvent of **9** under vacuum, the residue was dissolved in CH_2Cl_2 and layered with CH_3CN. After storage at room temperature for one day dark red-brown plates of **9** were obtained. The supernatant was decanted off, the crystals were washed with CH_3CN and dried under vacuum. Yield (**9**): 40 mg (40%).

Synthesis of 10: a) A solution of [Li(thf)$_4$][(Cp*Fe)(η⁴-P_5tBu)] (100 mg, 0.1432 mmol, 2 equiv.) in thf was cooled to -80 °C and a solution of [(Cp'''CoCl)$_2$] (47 mg, 0.0716 mmol, 1 equiv.) in thf was added. The reaction mixture was warmed to room temperature while the color changed from brown to red. The solvent was removed under vacuum, the residue extracted with hexane and filtered over diatomaceous earth. The solvent was removed under vacuum, the residue dissolved in CH_2Cl_2 and layered with acetonitrile. After a few days of storage at room temperature, [(Cp*Fe)(Cp'''Co)(μ,η⁴:η²:η¹-P_5tBu)] (**10**) could be obtained in form of dark blocks. The supernatant was decanted off and the crystals dried under vacuum. Yield (**10**): 48 mg (48%). b) A solution of $AgBF_4$ (35 mg, 0.18 mmol, 1 equiv.) in thf was added to a stirred solution of [Li(crypt)][(Cp*Fe)(Cp'''Co)(μ,η⁴:η²:η¹-P_5tBu)] (200 mg, 0.18 mmol, 1 equiv.) in thf. After stirring overnight, the formation of an Ag mirror on the Schlenk wall was observed. The solvent was removed under vacuum, the residue extracted with hexane and filtered over diatomaceous earth. After removal of the solvent under vacuum, the residue was dissolved in CH_2Cl_2 and layered with CH_3CN. After a few days dark blocks of [(Cp*Fe)(Cp'''Co)(μ,η⁴:η²:η¹-P_5tBu)] (**10**) were obtained. The supernatant was decanted off and the crystals dried under vacuum. The performed ^{1}H NMR experiment and X-band EPR experiment (solid and solution) matches the spectroscopic data of method a). Yield (**10**): 38 mg (30%).

Synthesis of 11: a) A solution of [Li(dme)$_3$][(Cp*Fe)(η⁴-P_5Me)] (100 mg, 0.1567 mmol, 2 equiv.) in thf was cooled to −80 °C and a solution of [(Cp'''CoCl)$_2$] (51.3 mg, 0.07835 mmol, 1 equiv.) in thf was added. The reaction mixture was warmed to room temperature while the color changed from brown to red. The solvent was removed under vacuum, the residue extracted with hexane and filtered over diatomaceous earth. The solvent was removed under vacuum, the residue dissolved in Et_2O and transferred into a double Schlenk with a small amount of toluene on the second side. After a few days at room temperature, [(Cp*Fe)$_2$(Cp'''Co)$_2$(μ$_4$,η⁴:η⁴:η²:η²η¹:η¹-$P_{10}Me_2$)] (**11**) crystallizes in form of dark blocks. The supernatant was decanted off and the crystals dried under vacuum. Yield (**11**): 252 mg (76%). b) A solution of [(Cp*Fe)(Cp'''Co)(μ,η⁴:η³-P_5)] (0.2 g, 0.313 mmol, 1 equiv.) in thf was cooled to -80 °C and MeLi (0.19 mL, 0.313 mmol, 1.6 mol/L in hexane, 1 equiv.) was added. The reaction mixture was warmed to room temperature while the color changed from violet to red. Then a solution of $AgBF_4$ (61 mg, 0.313 mmol, 1 equiv.) in thf was added and the color changed to red brown under the formation of an Ag mirror on the glass wall. The reaction mixture was stirred overnight. The solvent was removed under vacuum, the residue extracted with hexane and filtered over diatomaceous earth. The solvent was removed under vacuum. Dissolving the residue in CH_2Cl_2 and layering with acetonitrile or gas phase diffusion of an Et_2O solution into toluene (double Schlenk) did not yield any crystals. Therefore, the solvent was removed under vacuum and the dark brown residue dissolved in C_6D_6. ^{31}P{^{1}H} and ^{31}P NMR spectroscopy confirms the formation of [(Cp*Fe)$_2$(Cp'''Co)$_2$(μ$_4$,η⁴:η⁴:η²:η²η¹:η¹-$P_{10}Me_2$)] (**11**) as well as unidentified by-products.

Synthesis of 12: A solution of $KPPh_2$ in dme (6.75 mL, 0.2325 mol/L, 1.57 mmol, 1 equiv.) was added to a stirred solution of [(Cp*Fe)(Cp'''Co)(μ,η⁴:η³-P_5)] (1 g, 1.57 mmol, 1 equiv.) in thf at -80 °C. The color changed from dark red to brown. The reaction mixture was warmed to room temperature, while the color changed to green. A solution of $AgBF_4$ (306 mg, 1.57 mmol, 1 equiv.) in thf was added and the color changed to red brown under the formation of an Ag mirror on the glass wall. The reaction mixture was stirred overnight. The solvent was removed under vacuum, the residue extracted with hexane and filtered over diatomaceous earth. The solvent was removed under vacuum. The residue was dissolved in CH_2Cl_2, layered with acetonitrile, and stored at room temperature. After a few days, [(Cp*Fe)(Cp'''Co)(μ,η⁴:η²:η¹-P_6Ph_2)] (**12**) crystallizes as dark brown blocks. The supernatant was decanted off and the obtained crystals dried under vacuum. Yield (**12**): 91 mg (7%).

Synthesis of 13: [K(2,2,2-crypt)][(Cp*Fe)(Cp'''Co)(μ,η²:η¹:η⁴-P_6Ph_2)] (100 mg, 0.080 mmol, 1 equiv.) and $AgBF_4$ (15.6 mg, 0.080 mmol, 1 equiv.) were weighed in together and dme was added. After a few minutes a dark brown solid and a silver mirror were obtained. After stirring overnight, it was filtered over diatomaceous earth. The solvent was removed under vacuum. The residue was dissolved in CH_2Cl_2 and Ag[FAl] (119 mg, 0.080 mmol, 1 equiv.) in CH_2Cl_2 was added and a red to brown solution with a dark precipitate (Ag^0) was obtained. After stirring overnight, it was filtered over diatomaceous earth. The solvent was reduced, layered with hexane, and stored at −30 °C. After a few days, [(Cp*Fe)(Cp'''Co)(μ,η³:η²:η²:η¹-P_6Ph_2)][FAl] (**13**) crystallizes as dark brown needles. The supernatant was decanted off, the crystals washed with hexane and dried under vacuum. Due to the high sensitivity of this compound, it is not fully characterized. Even in the ^{1}H NMR spectrum of freshly prepared samples, decomposition products were observed. By NMR spectroscopy (see Figure S40 to Figure S42.) and X-band EPR spectroscopy (see Supporting Information Section 3.3) [(Cp*Fe)(Cp'''Co)(μ,η⁵:η⁵-P_5)][FAl] was characterized as one decomposition product.[27] Yield (**13**): 94 mg (53%).

Synthesis of 14: A solution of Ag[FAl] (100 mg, 0.067 mmol, 1 equiv.) in CH_2Cl_2 was added at to a solution of [(Cp*Fe)(Cp'''Co)(μ,η⁴:η²:η¹-P_5tBu)] (47 mg, 0.067 mmol, 1 equiv.) in CH_2Cl_2. The reaction mixture was stirred overnight and the color changed to violet under the formation of an Ag mirror on the glass wall and a dark precipitate. After stirring overnight, it was filtered via cannula. The solvent was reduced, layered with hexane, and stored at −30 °C. After one day, [(Cp*Fe)(Cp'''Co)(μ,η⁵:η⁴-P_5tBu)][FAl] (**14**) crystallizes as dark violet plates, which were separated under the microscope from a few colorless blocks. The crystals were washed with hexane (10 mL) five times and dried under vacuum. Yield (**14**): 55 mg (39%).

DFT calculations: The Gaussian 09 program[32] was used for all calculations. Density functional theory (DFT) in form of BP86[18,19] (Becke's exchange and Perdew 86 correlation functional) with TZVP basis set was employed. Natural bond orbital (NBO) analysis has been performed with the NBO6 program at the BP86/TZVP[33] (**2**–**14**) or BP86-D3BJ/def2-TZVP[34] (**1**, **2**, **4**, **5**, monomeric **11**) Wiberg Bond Indices (WBI) have been obtained from the calculations at the BP86/TZVP level of theory. Long range empirical dispersion

correction in form of GD3JB[35] was applied. For calculation of the cations (**2**, **4**, **5**, **6**) the dielectric constant of thf was used (ε = 7.4257) and for the cations (**13**, **14**) the dielectric constant of dichloromethane (ε = 8.93) was used. Electrostatic potential calculations were performed with D3BJ correction and implicit solvation model (SCRF = thf). Figures concerning the DFT calculations for the Supporting Information were created with Chemcraft[36] (spin density, optimized geometries) or Gaussian 09 (electrostatic potential).

Crystallographic Data: Deposition Number(s) 2207484 (**2**), 2207485 (**3**), 2207486 (**4**), 2207487 (**5**), 2207488 (**6**), 2207489 (**7**), 2207490 (**8**), 2207491 (**9**), 2207492 (**10**), 2207493 (**11**), 2207494 (**12**), 2207495 (**13**) and 2207496 (**14**) contain(s) the supplementary crystallographic data for this paper. These data are provided free of charge by the joint Cambridge Crystallographic Data Centre and Fachinformationszentrum Karlsruhe Access Structures service.

Analytical data, quantum chemical calculations and X-ray crystallography are described in the Supporting Information.

Acknowledgements

The Deutsche Forschungsgemeinschaft (DFG) is gratefully acknowledged for the support within the projects Sche 384/36-2 and Sche 384/38-3. Open Access funding enabled and organized by Projekt DEAL.

Conflict of Interest

The authors declare no conflict of interest.

Data Availability Statement

The data that support the findings of this study are available in the supplementary material of this article.

Keywords: functionalization · heterobimetallic complexes · organophosphorus ligands · oxidation · rearrangement

[1] a) A. Seitz, G. Balázs, M. Scheer, *Chem. Rev.* **2010**, *110*, 4236; b) D. J. Scott, J. Cammarata, M. Schimpf, R. Wolf, *Nat. Chem.* **2021**, *13*, 458; c) M. Donath, K. Schwedtmann, T. Schneider, F. Hennersdorf, A. Bauzá, A. Frontera, J. J. Weigand, *Nat. Chem.* **2022**, *14*, 384; d) M. B. Geeson, C. C. Cummins, *Chem. Sci.* **2020**, *6*, 848.
[2] B. M. Cossairt, N. A. Piro, C. C. Cummins, *Chem. Rev.* **2010**, *110*, 4164.
[3] M. Caporali, L. Gonsalvi, A. Rossin, M. Peruzzini, *Chem. Rev.* **2010**, *110*, 4178.
[4] M. Seidl, G. Balázs, M. Scheer, *Chem. Rev.* **2019**, *119*, 8406.
[5] C. M. Hoidn, D. J. Scott, R. Wolf, *Chem. Eur. J.* **2021**, *27*, 1886.
[6] a) P. Coburger, J. Leitl, D. J. Scott, G. Hierlmeier, I. G. Shenderovich, E. Hey-Hawkins, R. Wolf, *Chem. Sci.* **2021**, *12*, 11225; b) L. Giusti, V. R. Landaeta, M. Vanni, J. A. Kelly, R. Wolf, M. Caporali, *Coord. Chem. Rev.* **2021**, *441*, 213927; c) C. Gendy, J. Valjus, H. M. Tuononen, R. Roesler, *Angew. Chem. Int. Ed.* **2022**, *61*, e202115692.
[7] S. Reichl, E. Mädl, F. Riedlberger, M. Piesch, G. Balázs, M. Seidl, M. Scheer, *Nat. Commun.* **2021**, *12*, 5774.
[8] a) M. Peruzzini, R. R. Abdreimova, Y. Budnikova, A. Romerosa, O. J. Scherer, H. Sitzmann, *Organometallics* **2004**, *689*, 4319; b) G. Capozzi, L. Chiti, M. Di Vaira, M. Peruzzini, P. Stoppioni, *J. Chem. Soc., Chem. Commun* **1986**, 1799.
[9] a) E. Mädl, G. Balázs, E. Peresypkina, M. Scheer, *Angew. Chem. Int. Ed.* **2016**, *55*, 7702; b) for electrophilic functionalization cf.: Ch. Riesinger, L. Dütsch, G. Balázs, M. Bodensteiner, M. Scheer, *Chem. Eur. J.* **2020**, *26*, 17166.
[10] A. Cavaille, N. Saffon-Merceron, N. Nebra, M. Fustier-Boutignon, N. Mezailles, *Angew. Chem. Int. Ed.* **2018**, *57*, 1874.
[11] M. Piesch, M. Seidl, M. Scheer, *Chem. Sci.* **2020**, *11*, 6745.
[12] M. Piesch, S. Reichl, M. Seidl, G. Balázs, M. Scheer, *Angew. Chem. Int. Ed.* **2021**, *60*, 15101.
[13] C. Riesinger, G. Balázs, M. Seidl, M. Scheer, *Chem. Sci.* **2021**, *12*, 13037.
[14] E. Mädl, M. V. Butovskii, G. Balázs, E. Peresypkina, A. V. Virovets, M. Seidl, M. Scheer, *Angew. Chem. Int. Ed.* **2014**, *53*, 7643.
[15] E. Mädl, E. Peresypkina, A. Y. Timoshkin, M. Scheer, *Chem. Commun.* **2016**, *52*, 12298.
[16] M. Piesch, F. Dielmann, S. Reichl, M. Scheer, *Chem. Eur. J.* **2020**, *26*, 1518.
[17] M. Piesch, M. Scheer, *Organometallics* **2020**, *39*, 4247.
[18] A. D. Becke, *Phys. Rev. A.* **1988**, 3098.
[19] J. P. Perdew, *Phys. Rev. B.* **1986**, 8822.
[20] For R = *t*Bu also single crystals of the oxidized product [Li(2,2,2-crypt)][(Cp*Fe)(Cp‴Co)(μ,η^4:η^3-P$_5$)] as well as [Li(opened-2,2,2-crypt)][(Cp*Fe)(Cp‴Co)(μ,η^4:η^2:η^1-P$_5$*t*Bu)], where the cryptand molecule did undergo ring-opening, were obtained and separated under the microscope to give analytically pure **2**.
[21] P. Pyykkö, M. Atsuni, *Chem. Eur. J.* **2009**, *15*, 186.
[22] P. Pyykkö, M. Atsuni, *Chem. Eur. J.* **2009**, *15*, 12770.
[23] C. G. P. Ziegler, T. M. Maier, S. Pelties, C. Taube, F. Hennersdorf, A. W. Ehlers, J. J. Weigand, R. Wolf, *Chem. Sci.* **2019**, *10*, 1302.
[24] O. J. Scherer, T. Völmecke, G. Wolmershäuser, *Eur. J. Inorg. Chem.* **1999**, 945.
[25] O. J. Scherer, B. Höbel, G. Wolmershäuser, *Angew. Chem. Int. Ed. Engl.* **1992**, *31*, 1027.
[26] M. V. Butovskii, G. Balázs, M. Bodensteiner, E. Peresypkina, A. V. Virovets, J. Sutter, M. Scheer, *Angew. Chem. Int. Ed.* **2013**, *52*, 2972.
[27] M. Piesch, *PhD thesis*, University of Regensburg, **2020**.
[28] O. J. Scherer, T. Brück, *Angew. Chem.* **1987**, *99*, 59.
[29] F. Baumann, E. Dormann, Y. Ehleiter, W. Kaim, J. Kärcher, M. Kelemen, R. Krammer, D. Saurenz, D. Stalke, C. Wachter, G. Wolmershäuser, H. J. Sitzmann, *J. Organomet. Chem.* **1999**, *587*, 267.
[30] T. Köchner, N. Trapp, A. J. Engesser, C. Röhr, S. Riedel, C. Knapp, H. Scherer, I. Krossing, *Angew. Chem. Int. Ed.* **2011**, *50*, 11253.
[31] Even using isolated **4** for the quenching with MeI did not improve the yield of **7**.
[32] M. J. Frisch, G. W. Trucks, H. B. Schlegel, G. E. Scuseria, M. A. Robb, J. R. Cheeseman, G. Scalmani, V. Barone, B. Mennucci, G. A. Petersson et al., *Gaussian, Inc.*, Wallingford CT, **2013**.
[33] *NBO 6.0*, Glendening, E. D.; Badenhoop, J. K.; Reed, A. E.; Carpenter, J. E.; Bohmann, J. A.; Morales, C. M.; Landis, C. R.; Weinhold, F., Theoretical Chemistry Institute of Wisconsin, Madison, WI, **2013**.
[34] a) F. Weigend, R. Ahlrichs, *Phys. Chem. Chem. Phys.* **2005**, *7*, 3297; b) F. Weigend, *Phys. Chem. Chem. Phys.* **2006**, *8*, 1057.
[35] a) S. Grimme, J. Antony, S. Ehrlich, H. Krieg, *J. Chem. Phys.* **2010**, *132*, 154104; b) S. Grimme, S. Ehrlich, L. Goerigk, *J. Comb. Chem.* **2011**, *32*, 1456.
[36] G. A. Zhurko, *Chemcraft - graphical program for visualization of quantum chemistry computations. https://chemcraftprog.com.*.

Manuscript received: February 13, 2023
Accepted manuscript online: March 16, 2023
Version of record online: ■■, ■■

RESEARCH ARTICLE

Various transformations of the initial *cyclo*-P_5 ligand in the triple-decker complex [(Cp*Fe)(Cp'''Co)($\mu,\eta^5:\eta^4$-P_5)] show that the reaction with main group nucleophiles yields different products depending on the steric demand of the nucleophile used. Subsequent oxidation/electrophilic quenching provides a plethora of P_5R_2 and P_6R_3 organophosphorus ligand complexes in unique 1,3 or 1,4 substitution pattern as opposed to the parent complex [Cp*Fe(η^5-P_5)].

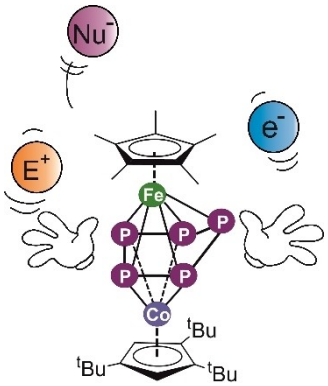

*S. B. Dinauer, Dr. M. Piesch, R. Szlosek, Dr. M. Seidl, Dr. G. Balázs, Prof. Dr. M. Scheer**